PCCP

PAPER

View Article Online
View Journal | View Issue



Cite this: *Phys. Chem. Chem. Phys.*, 2014, **16**, 13103

# A study on the versatility of metallacycles in host–guest chemistry: Interactions in halide-centered hexanuclear copper(II) pyrazolate complexes†

Miguel Ponce-Vargas[a] and Alvaro Muñoz-Castro*[ab]

Received 22nd March 2014,
Accepted 4th May 2014

DOI: 10.1039/c4cp01238k

www.rsc.org/pccp

Hexanuclear copper(II) pyrazolate complexes have shown the ability to encapsulate different halide ions, leading to [*trans*-$Cu_6\{\mu$-3,5-$(CF_3)_2pz\}_6(\mu$-$OH)_6X]^-$ (X = F, Cl, Br, I). They offer an interesting case study for variation in local properties at host binding sites, due to the presence of a six membered ring involving Cu(II) centers considered as the borderline Lewis acid according to the Pearson Hard and Soft Acids and Bases (HSAB) principle. Here, we describe the host–guest interactions *via* relativistic density functional calculations, involving the graphical description of local dipole and quadrupole moments, energy decomposition analysis, non-covalent indices, and magnetic behavior. The observed variation in the copper local dipole and quadrupole moments suggests that a metallacycle host offers great advantages in comparison to their organic counterparts, prompted by the versatility of the metallic centers to modulate the surrounding electron density accordingly. According to our results, the contribution of ion–dipole forces in the halide-centered series decreases from 95.0% to 77.0% from the fluoride to the iodide complex, whereas the contribution of higher order interactions such as quadrupole–dipole and quadrupole–quadrupole, goes from 5.0% to 23.0% towards a softer guest. In addition, the through-the-space magnetic response of *trans*-$Cu_6\{\mu$-3,5-$(CF_3)_2pz\}_6(\mu$-$OH)_6$, reveals a noteworthy aromatic structure, which is driven by the superexchange through the ligands leading to a singlet ground state.

## Introduction

The term 'metallacycle' is generally used to refer to any cyclic framework with at least one metallic center involved.[1] These systems offer interesting properties based on their unique structures, and the ability to incorporate several guest species. Thus, they represent a step forward in fields such as molecular recognition,[2] catalysis,[3,4] molecular magnetism,[5] and biomedicine,[6] among others. Metallacycles acting as host species, allow organic compounds[7,8] and multiple ions[9,10] to be incorporated into their structures mainly *via* long-range non-covalent interactions (van der Waals forces). Usually, the host moiety interacts with the guest through the oxygen or nitrogen atoms located within the supporting ligands;[11–14] whereas, to a lesser extent, the metallic centers within the host structure play this role offering a more interesting scenario driven by the versatility of a discrete number of redox centers in a single molecular entity.[15,16]

In this concern, we focus on the series of halide-centered hexanuclear anionic copper(II) pyrazolate complexes [*trans*-$Cu_6\{\mu$-3,5-$(CF_3)_2pz\}_6(\mu$-$OH)_6X]^-$, where X = F, Cl, Br, I, characterized by Mohamed and coworkers,[17] since they represent an interesting case study to evaluate the host–guest capabilities involving a multimetallic array. Such systems are based on a ring consisting of six copper(II) centers interacting with different halide ions of increasing size, depicting a highly symmetric structure ($D_{3d}$). The metallic centers are bridged by six hydroxyl groups and six pyrazolate ligands arranged alternately, denoting a local square planar coordination geometry in each copper site. The resulting cavity size allows the inclusion of a halide ion into the center of the metallacycle array, as has been described by the authors.[17] The $Cu_6$ ring is formed by Cu(II) ions, which are borderline Lewis acids under the Pearson Hard and Soft Acid–Base (HSAB) principle, which interact with $F^-$, $Cl^-$, $Br^-$ and $I^-$, considered as hard, intermediate and soft Lewis bases.[26]

The affinity of a host for a given guest depends on the shape, size, conformation, and surface charge distribution of the moieties,[18] where non-covalent interactions such as dispersion forces, play a crucial role in organizing the supramolecular structure.[19] As these forces are related to electronic-density distribution surrounding the host–guest pair nuclei, the theoretical

[a] *Doctorado en Fisicoquímica Molecular, Universidad Andres Bello, República 275, Santiago, Chile*
[b] *Dirección de Postgrado e Investigación, Universidad Autonoma de Chile, Carlos Antúnez 1920, Santiago, Chile. E-mail: alvaro.munoz@uautonoma.cl*

† Electronic supplementary information (ESI) available. See DOI: 10.1039/c4cp01238k

description of the local quadrupole moments at such nuclei is of great interest in order to obtain a deeper rationalization of the host–guest phenomenon.[20,21] Usually dispersion interactions are evaluated according to the widely employed pairwise Grimme correction,[22] which is subsequently included by adding an attractive energy term summed over all atomic pairs in the system. The parameterization of this method is still an active field of research.[23]

Under this framework, we suggest that a reasonable way to understand the different types of interactions governing the host–guest formation is given by the study of the quadrupole moment tensors located at the binding sites. Such property provides information about the electronic-density departure and atomic polarizability experienced at the relevant sites of the metallacycle complexes. The atomic quadrupole moments ($\Theta$) can be obtained from the method developed by Swart and co-workers, where a charge analysis derived from an atomic multipole expansion allow us to access not only molecular quadrupole moments, but also local atomic quadrupoles.[24] The anisotropies of such quantities are associated with electron density fluctuations, responsible for non-covalent interactions. Taking advantage of this, it is possible to gain insights into the interaction pattern *via* the graphical projection of the quadrupole moments through a spatial representation of the quadrupole tensors, providing deeper insights into the formation of the host–guest pair.[25,26]

The aim of this work is to gain a deeper understanding of non-covalent forces in hexanuclear copper(II) pyrazolate complexes by using DFT methodologies, where the nature of the guest, according to the HSAB principle, goes from a hard to a soft Lewis base. The host–guest interaction strength is evaluated according to the Ziegler–Morokuma energy partitioning scheme including the dispersion term in line with the pairwise Grimme approach.[22] The graphical representation of the regions displaying the host–guest interaction was obtained according to the non-covalent interaction (NCI)[27] analysis. Lastly, the through-the-space magnetic response of *trans*-$Cu_6\{\mu\text{-}3,5\text{-}(CF_3)_2pz\}_6(\mu\text{-}OH)_6$ is obtained in order to generate a representation map of this highly sensitive property denoting the consequence given by the guest inclusion into the metallacycle host.

## Computational details

Relativistic density functional theory[28] calculations were done by using the ADF 2012 code,[29] *via* the scalar ZORA Hamiltonian. An all electron triple-$\xi$ Slater basis set plus polarization function (STO-TZP) was employed within the meta-generalized gradient approximation (meta-GGA) of Tao, Perdew, Staroverov, and Scuseria (TPSS)[30] and the GGA approximation of Perdew, Burke, and Ernzerhof (PBE). The performance of the TPSS functional has been evaluated in the calculation of dissociation energies and geometries of hydrogen-bonded complexes,[31] binding energies of transition metal dimers,[32] and excitation energies of small molecules and atoms.[33] Geometry optimizations were done *via* the analytical energy gradient method implemented by Verluis and Ziegler.[34]

The dispersion Grimme correction[22] was added in order to account for long-range interactions. The strong antiferromagnetic coupling observed for the copper centers inside the [*trans*-$Cu_6\{\mu\text{-}3,5\text{-}(CF_3)_2pz\}_6(\mu\text{-}OH)_6Cl]^-$ and [*trans*-$Cu_6\{\mu\text{-}3,5\text{-}(CH_3)_2pz\}_6(\mu\text{-}OH)_6\cdot CH_3CN\cdot CHCl_3$] structures,[8] allows us to consider only the singlet state form of the studied systems.[35]

The calculation of atomic quadrupole moments ($\Theta$) is conducted in three stages: first, the molecular charge density is expressed as a sum of atomic densities, then from these atomic densities a set of atomic multipoles is defined and then used to obtain the electrostatic potential outside the charge distribution, finally these atomic multipoles are reconstructed by using a scheme that distributes charges over all atoms to reproduce the multipoles exactly.[24] The values of $\Theta$ were obtained from a single-point calculation at the optimized geometries, neglecting any symmetry operation leading to the $C_1$ point group. Then, the graphical representation of the atomic quadrupole tensors was obtained based on the method employed by Autschbach and coworkers,[36] considering a function written in spherical coordinates representing the expression, $f(r) = \Sigma_{jk} r_j r_k \Theta_{jk}$, centered at the respective nuclei, thus obtaining a surface representation of the angular dependence $\Theta_{jk}$.[37] All tensors were plotted by using the Chemcraft software.[38]

The non-covalent interaction (NCI) analysis was carried out by using the NCIPLOT program developed by Weitao Yang and coworkers[27] and the NCI Milano program developed by Saleh and coworkers,[39,40] both based on the analysis of electron density descriptors. The NCI isosurfaces have been plotted using the Visual Molecular Dynamics (VMD) software.[41]

The through-the-space magnetic response has been obtained by mapping the molecular shielding tensor[42] at several nuclear independent points in the molecular domain, within the GIAO formalism, employing the GGA exchange expression proposed by Handy and Cohen[43] and the correlation expression proposed by Perdew, Burke, and Ernzerhof[44] (OPBE), incorporating the scalar relativistic corrections (OPBE/ZORA).

## Results and discussion

### Structural parameters

The calculated structure for *trans*-$Cu_6\{\mu\text{-}(3,5\text{-}(CF_3)_2pz)\}_6(\mu\text{-}OH)_6$ (**1**) is shown in Fig. 1. To the best of our knowledge, this cyclic structure without a guest has not been isolated until now. Recently, Cañón-Mancisidor and coworkers obtained the isostructural metallacycle [*trans*-$Cu_6\{\mu\text{-}3,5\text{-}(CH_3)_2pz\}_6(\mu\text{-}OH)_6\cdot CH_3CN\cdot CHCl_3$].[8] In *trans*-$Cu_6\{\mu\text{-}(3,5\text{-}(CF_3)_2pz)\}_6(\mu\text{-}OH)_6$, each Cu(II) has a local square planar geometry, and the pyrazolate anions alternate positions with the μ-OH moieties above and below the plane generated by the six Cu(II) ions resulting in a structure that belongs to the $D_{3d}$ symmetry group. The expected high spin metallacycle involving six paramagnetic centers is quenched by a strong antiferromagnetic coupling within the host structure.[8,17]

The host–guest systems involve the formation of halide-centered[17] metallacycles derived from **1**, namely, **1**-F, **1**-Cl, **1**-Br and **1**-I. Selected distances and angles for the host and the halide-centered copper(II) pyrazolate complexes are given in

 

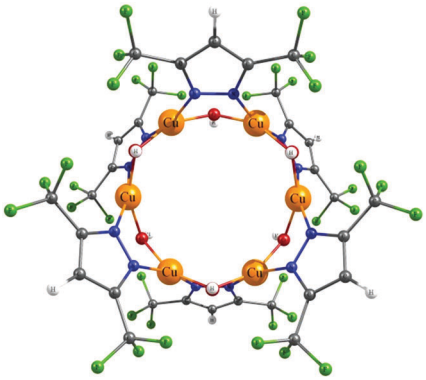

Fig. 1 Optimized structure for *trans*-$Cu_6\{\mu\text{-}3,5\text{-}(CF_3)_2pz\}_6(\mu\text{-}OH)_6$, viewed from the *z*-axis. Color code: Cu orange, N blue, C grey, and F green.

Table 1, which are compared to the available structural data for **1**-Cl, **1**-Br and **1**-I.[17] The calculated bond distances for the complexes are in good agreement with experimental data,[17] suggesting that methods used here are reliable for optimizing the molecular geometries of these systems. Similar results have been obtained at the PBE/ZORA and TPSS/ZORA levels, thus hereafter all the calculated data refer to the latter level of theory. All the optimized structures belong to the $D_{3d}$ symmetry point group, denoting Cu–Cu bond distances of about ~3.1 Å, which are out of the van der Waals radii sum range (2.8 Å).[45] This point suggests a negligible direct Cu–Cu interaction, thus the stabilization of the $Cu_6$-based structure is given mainly by the pyrazolate and hydroxyl bridging ligands.

The diameter depicted by the $Cu_6$ ring including the halide guest, ranges from 6.145 to 6.247 Å, which is contracted with respect to **1** (6.373 Å) due to the host–guest pair interaction. With the incorporation of the guest, the dihedral angle between the $Cu_6$ and Cu–O–Cu planes increases from 115° to about 122° probably due to steric repulsion forces between the oxygen atoms and the guest. However, the distance between the center of the cavity and the hydrogens belonging to the μ-OH groups, remains almost unaltered, which could be attributed to hydrogen-bond forces established between the halide guest and the hydroxyl groups. Furthermore, the increase of the ($Cu_6$)–(Cu–O–Cu) dihedral angle described above (Table 1), could be related to repulsion forces between the electron-rich oxygen atoms and the axial component of the guest quadrupole (see below) as a result of the guest entry.

### Host–guest interaction

According to the Morokuma–Ziegler scheme[46,47] the energy decomposition analysis (EDA) was employed in order to obtain a suitable description of terms contributing to the host–guest coupling forces, and how they evolve along the studied series. Under this scheme, the total interaction energy ($\Delta E_{int}$) can be decomposed into three main components, namely, $\Delta E_{elec}$, $\Delta E_{Pauli}$ and $\Delta E_{orb}$. The first term is computed by considering each fragment (namely, A and B) in its unperturbed (frozen) electron density as an isolated species ($\Psi_A\Psi_B$). The $\Delta E_{Pauli}$ term comprises the destabilizing four-electron two-orbital interactions between occupied orbitals, which is calculated from the energy change upon antisymmetrization and renormalization of the overlapped fragment densities ($\Psi^0 = N\hat{A}\{\Psi_A\Psi_B\}$). Lastly, the $\Delta E_{orb}$ term is obtained when the densities are allowed to relax into the final molecular orbitals ($\Psi_{AB}$). The $\Delta E_{elec}$ term accounts for the stabilizing electrostatic interaction, whereas $\Delta E_{orb}$ stands for the stabilizing covalent character and polarization of the host–guest interactions due to a charge transfer from guest occupied orbitals towards the host empty ones. Lastly, the $\Delta E_{Pauli}$ term describes the Pauli pair repulsion. Moreover, the stabilizing electrostatic term involves the contribution from electrostatic ion–dipole, dipole–dipole, dipole–quadrupole, quadrupole–quadrupole interactions, *etc.* To overcome the basis set superposition error (BSSE), the counterpoise method[47] was employed denoting BSSE values of about 1.5 kcal $mol^{-1}$. The results of the EDA analysis including the Grimme dispersion correction and the counterpoise correction are summarized in Table 2.

The calculated data suggest that $\Delta E_{elec}$ represents about 70% of the total stabilization energy, playing a more important role than the orbital interaction (~20%), thus, revealing the electrostatic character of the host–guest coupling. This behavior can be attributed to the relevance of the ion–dipole, quadrupole–dipole and quadrupole–quadrupole interactions between the guest and the binding site of the host, namely the Cu(II) centers, resulting in the stabilization of the host–guest pair. In addition, the dispersion contribution to the host–guest couple stabilization increases to about 5%.

According to the guest, the local dipole moment ($\mu$) located at each Cu(II) site increases from 0.040 Debye (D) for **1** to 0.094 D for **1**-F, < 0.174 D for **1**-Cl, < 0.207 D for **1**-Br and < 0.343 D for **1**-I, denoting the variation range for the binding sites located at the host contributing to the ion–dipole and quadrupole–dipole host–guest interactions. In all cases the

Table 1 Selected distances (Å) and angles (degrees) of the host and $Cl^-$, $Br^-$ and $I^-$ complexes

| | **1** | **1**-F | **1**-Cl | | **1**-Br | | **1**-I | |
|---|---|---|---|---|---|---|---|---|
| | Calc. | Calc. | Exp.[a] | Calc. | Exp.[a] | Calc. | Exp.[a] | Calc. |
| Diam. $Cu_6$ | 6.373 | 6.149 | 6.057 | 6.145 | 6.088 | 6.153 | 6.195 | 6.247 |
| Cu–Cu | 3.187 | 3.074 | 3.071 | 3.073 | 3.075 | 3.076 | 3.088 | 3.123 |
| Cu···center | 3.187 | 3.074 | 3.068 | 3.073 | 3.043 | 3.076 | 3.098 | 3.123 |
| H···center | 3.599 | 3.339 | 4.140 | 3.431 | 3.417 | 3.455 | 3.461 | 3.514 |
| ⟨($Cu_6$)–(Cu–N–N–Cu) | 117° | 117° | 117° | 118° | 116° | 118° | 116° | 118° |
| ⟨($Cu_6$)–(Cu–O–Cu) | 115° | 115° | 123° | 121° | 124° | 122° | 124° | 123° |

[a] Experimental data from ref. 17.

Table 2 Energy decomposition analysis (EDA, kcal mol$^{-1}$) and natural population analysis (NPA, a.u.) of the studied systems

| | **1** | **1**-F | | **1**-Cl | | **1**-Br | | **1**-I | |
|---|---|---|---|---|---|---|---|---|---|
| EDA | | | | | | | | | |
| $\Delta E_{orb}$ | | −34.15 | 35.6% | −32.6 | 24.8% | −33.28 | 20.1% | −37.73 | 17.6% |
| $\Delta E_{elec}$ | | −57.34 | 59.9% | −91.09 | 69.4% | −123.24 | 74.3% | −165.45 | 77.2% |
| $\Delta E_{disp}$ | | −4.3 | 4.5% | −7.54 | 5.8% | −9.25 | 5.6% | −11.04 | 5.2% |
| $\Delta E_{Pauli}$ | | 16.36 | | 58.23 | | 95.96 | | 154.1 | |
| $\Delta E_{int}$ | | −79.43 | | −73.00 | | −69.81 | | −60.12 | |
| NPA | | | | | | | | | |
| X | | −0.85 | | −0.88 | | −0.85 | | −0.80 | |
| [$Cu_6$] | 7.35 | 7.32 | | 7.59 | | 7.56 | | 7.49 | |
| L[a] | −3.92 | −3.83 | | −4.19 | | −4.19 | | −4.17 | |
| $(OH)_6$ | −3.43 | −3.30 | | −3.52 | | −3.52 | | −3.52 | |

[a] L = [3,5-$(CF_3)_2$pz]$_6$.

copper dipole moment points towards the guest, denoting that the ion–dipole interaction is located at the $Cu_6$ plane, as is represented in Fig. 2. Due to symmetry considerations given by the $D_{3d}$ point group, the halide guest does not exhibit a local dipole moment.

These results denote the versatility of the Cu(II) center to modulate its dipole moment towards the halide guest.

Our results suggest that the fluorine complex (**1**-F) is the most favorable structure (−79.4 kcal mol$^{-1}$) followed by the chloride (−73.0 kcal mol$^{-1}$), bromide (−69.8 kcal mol$^{-1}$) and iodide (−60.1 kcal mol$^{-1}$) complexes. This is in line with the destabilizing term ($\Delta E_{Pauli}$) related to the steric repulsion as a consequence of the guest size. The stabilization energy given by the dispersion term, increases within the series, where the iodide host–guest system (**1**-I) presents the largest dispersion energy term (−11.04 kcal mol$^{-1}$), followed by the bromide (−9.25 kcal mol$^{-1}$) and chloride (−7.54 kcal mol$^{-1}$) systems. This trend is in accordance with the inclusion of a softer guest species,[26] which is also accounted for the variation in the $\Delta E_{orb}$ term, which concerns the polarization of fragments due to electronic density relaxation given by the formation of the overall host–guest system. The inclusion of the solvation effect *via* a polarizable continuum model (conductor-like screening model, COSMO) varies the results discussed above to a small extent hence no further discussion is given.

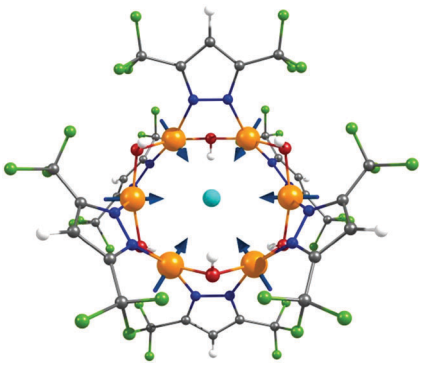

Fig. 2 Graphical representation of the copper dipole moments in [*trans*-$Cu_6${μ-3,5-$(CF_3)_2$pz}$_6$(μ-OH)$_6$Cl]$^-$.

According to the obtained interaction energies, [*trans*-$Cu_6$-{μ-3,5-$(CF_3)_2$pz}$_6$(μ-OH)$_6$] should exhibit a selectivity for the inclusion of differents halides, leading to preferences for hard bases.

With the aim of reducing the large contribution to the electrostatic term given by the ion–dipole interaction, allowing us to evaluate higher order interactions, such as quadrupole–dipole and quadrupole–quadrupole, we include the analysis of the hypothetically related noble-gas (Ng) pyrazolate complexes (Table S2, ESI†). Noble gases are isoelectronic with the corresponding halides, having similar sizes, and due to their closed-shell electronic configuration, they enable us to evaluate uncharged species directly related to **1**-F, **1**-Cl, **1**-Br and **1**-I, enabling electrostatic contribution of the ion–dipole term to be effectively reduced. The results obtained from the geometry optimizations and EDA analyses for such hypothetical structures are summarized in Tables S1 and S2 (ESI†).

In the **1**-Ng series (Table S3, ESI†), the electrostatic contribution decreases in a noteworthy manner to values in the range of −2.89 to −38.07 kcal mol$^{-1}$, in contrast to the halide case (−57.34 to −165.45 kcal mol$^{-1}$), which is attributed to the cancellation of the ion–dipole interaction leading to only quadrupole–dipole and quadrupole–quadrupole ones. The dispersion interaction energies in the **1**-Ng series remain almost unaltered; however their relative contribution represents about 27% of the stabilizing energy.

The comparison between the halide (**1**-X) and the neutral (**1**-Ng) series, allows us to characterize that the ion–dipole interaction contribution to the electrostatic term ranging from 95.0% to 77.0% ($1 - ({}^{Ng}\Delta E_{elec}/{}^{X}\Delta E_{elec})$) going from **1**-F to **1**-I, as it is obtained by the relationship between the $\Delta E_{elec}$ stabilizing terms in the noble-gas complexes and their respective halide systems. This fact allows us to conclude that the contribution from higher-order interactions such as quadrupole–dipole and quadrupole–quadrupole forces, increases from 5.0% to 23.0% according to the inclusion of hard, intermediate and soft Lewis bases[26] given by $F^-$, $Cl^-$, $Br^-$ and $I^-$.

In order to evaluate the charge distribution for **1**, and the halide counterparts leading to the host–guest couple, natural population analysis was carried out by using the stand-alone NBO5 suite. The inclusion of the halide guest gives rise to a small charge transfer (Table 2), leading to $\sim -0.8|e|$ charge at

 

Table 3 Principal components of the electronic quadrupole tensor of the studied systems, for a representative copper and guests (Buckinghams)

| | Cu | | | | X | | | |
|---|---|---|---|---|---|---|---|---|
| | $\Theta_{11}$ | $\Theta_{22}$ | $\Theta_{33}$ | $\Theta_{aniso}$ | $\Theta_{11}$ | $\Theta_{22}$ | $\Theta_{33}$ | $\Theta_{aniso}$ |
| **1** | 0.280 | 0.008 | −0.288 | −0.43 | — | — | — | — |
| **1**-F | 0.259 | −0.022 | −0.237 | −0.35 | 0.022 | 0.022 | −0.044 | −0.06 |
| **1**-Cl | 0.372 | −0.161 | −0.211 | −0.32 | 0.176 | 0.176 | −0.352 | −0.53 |
| **1**-Br | 0.401 | −0.167 | −0.233 | −0.35 | 0.118 | 0.118 | −0.236 | −0.35 |
| **1**-I | 0.553 | −0.160 | −0.393 | −0.59 | 1.297 | 1.297 | −2.594 | −3.89 |

the guest, which vary according to the trend of the $\Delta E_{orb}$ term. The distribution of the incoming charge into the host is mainly observed at the $Cu_6$ ring and pyrazolate derivatives, revealing the interplay between such fragments to modulate the structure in the formation of the complex. Thus, the interaction with a softer guest increases the contribution from higher order interactions.

To obtain a clear representation of the degree of departure from the spherical symmetry experienced by the electronic density at the guest and host binding sites, we evaluate the corresponding quadrupole moment tensors (Table 3), including their graphical representation as an isosurface, similarly to other second rank tensorial magnitudes.[48] The jk component of the quadrupole moment tensor is given by

$$\Theta_{jk} = \int \rho(r)\left(\frac{3}{2}r_j r_k - \frac{1}{2}\delta_{jk}\mathbf{r}^2\right)d\tau$$

where $\rho(r)$ is the total charge density of the atom or molecule, $\mathbf{r}$ is the vector which defines the position of the charge element $\rho(\mathbf{r})d\tau$, $r_j$ and $r_k$ denote, respectively, the j and k components of $\mathbf{r}$, and $d\tau$ is the volume differential. A set of principal axes can always be found such that off-diagonal elements vanish leading to the principal axis representation (PAS), where the tensor is depicted in its own framework. We designate the $\Theta_{jk}$ components, according to $\Theta_{11} > \Theta_{22} > \Theta_{33}$, in order to describe the more negative component by $\Theta_{33}$. The graphical representation of such quantities is given in Fig. 3, where positive values of $\Theta_{jk}$ describe positive electron-deficient regions, and negative values, electron-rich regions around the respective nucleus. Similar results have been obtained at the PBE/ZORA level (Tables S4 and S5, ESI†). Therefore, hereafter results refer to the results obtained at the TPSS/ZORA level.

In our particular case ($D_{3d}$ point group), the central guest describes the relationship given by $\Theta_{11} = \Theta_{22} \neq \Theta_{33}$, where the axial component ($\Theta_{33}$) exhibits negative values and the perpendicular components ($\Theta_{11}$ and $\Theta_{22}$) positive ones. This implies that the central guest quadrupole moment is distorted axially (Fig. 4, left), the electronic charge being removed from the plane containing the $\Theta_{11}$ and $\Theta_{22}$ components and concentrated along the main axis.[49] This observation accounts for the dipole–quadrupole host–guest interaction which occurs in the $Cu_6$ plane, in addition to the ion–dipole interaction.

In order to give a clear description of quadrupole moment departure from the spherical symmetry, we introduce the quadrupole anisotropic component ($\Theta_{aniso}$) in analogy to the

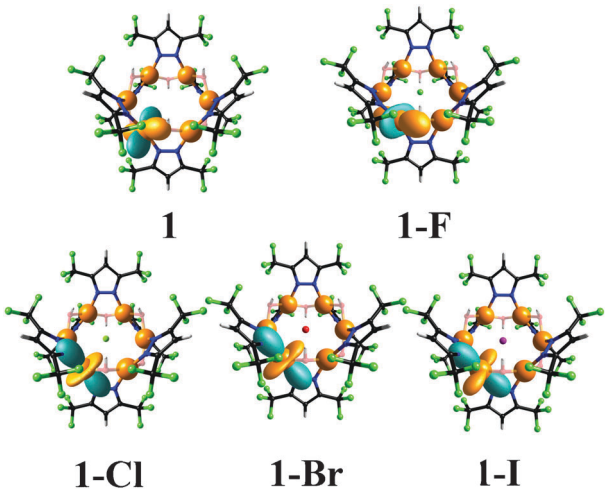


Fig. 3 Graphical representation of the local electric quadrupole tensor at the Cu(II) center (+/−: blue/orange).

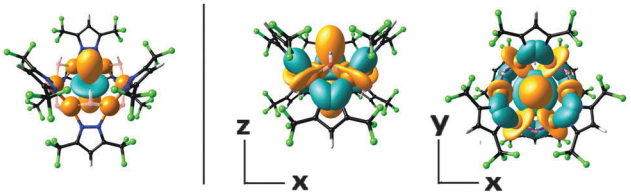


Fig. 4 Representative local electric quadrupole tensor of the guest for **1**-Cl, **1**-Br and **1**-I (left), denoting the match between the negative and positive lobes (two-views, right) between the Cu and X centers (+/−: blue/orange).

Haerberlen convention[50,51] employed in solid-state NMR experiments. Thus, $\Theta_{aniso}$ is defined by

$$\Theta_{aniso} = \Theta_{33} - \frac{(\Theta_{11} + \Theta_{22})}{2}$$

The more polarizable iodide guest consequently exhibits the larger $\Theta_{aniso}$, which accounts for the larger $\Delta E_{elec}$ term in the stabilization of the host–guest couple inside the series.

The atomic quadrupole moments exhibit interesting features, due to that **1** involves six Cu(II) centers considered as borderline Lewis acids in the Pearson Hard and Soft Acids and Bases (HSAB) principle, which experience different distribution of the surrounding electron density. Thus, each Cu(II) center can vary its quadrupole moment (Table 3) according to the involved guest, namely, $F^-$, $Cl^-$, $Br^-$ and $I^-$, which are considered as hard, intermediate and soft Lewis bases,[26] denoting the versatility provided by the inclusion of metallic centers as binding sites in the host structure. In Fig. 3, the variation in the $\Theta$ quantity can be seen for a representative Cu(II) center, given by the graphical representation of such second-rank tensor. For **1**, $\Theta$ is contained in mainly two principal axes given by $\Theta_{11}$ and $\Theta_{33}$ ($\Theta_{22} \approx 0$), the former oriented towards the center of the metallacycle (blue/+) and the latter along the Cu–O bond (orange/−). The latter ($\Theta_{33}$) follows the more electron-rich bond

at the local square planar geometry of Cu(II), which is represented by the negative lobes of the copper quadrupole tensor (orange color).

In the case of the host–guest complexes, $\Theta$ exhibits a different shape because the electron-rich region is located between the Cu–O and Cu–X bond distances (X = Cl, Br, I). Going from **1**-Cl to **1**-I, the $\Theta_{33}$ component is oriented in a large extent towards the Cu–X interaction, resulting in a negatively-charged region at the $Cu_6$ plane. The electro-positive component ($\Theta_{11}$, positive lobes) is oriented along the Cu–N bond, which leads to a positively charged region above and below the $Cu_6$ ring (Fig. 4). We suggest that these electron-deficient regions are those that mainly interact with the negative axial distribution of the guest, leading to quadrupole–quadrupole host–guest forces. $\Theta_{33}$ reaches its more negative values in the **1**-I case (Table 3), where a more effective match occurs between the guest axial component ($^{X}\Theta_{33}$) and the metallacycle electron deficient regions defined by the copper quadrupole positive lobes ($^{Cu}\Theta_{11}$). Thus, this methodology gives a clear description of quadrupole–quadrupole host–guest forces which are mainly located above and below the $Cu_6$ plane, in contrast to the ion–dipole and quadrupole–dipole interactions which are contained in the $Cu_6$ plane.

The copper sites at the metallacrown framework, exhibit different amounts of distortion of their quadrupole moment ($\Theta_{aniso}$), which are related to the increase of the stabilizing terms enabling to overcome the steric repulsion term ($\Delta E_{Pauli}$), resulting in a favorable host–guest coupling (Table 2). The study of the hypothetical uncharged counterparts reveals a different tensor shape which is retained for **1**-Ne, **1**-Ar, **1**-Kr and **1**-Xe (Fig. S1, ESI†), where the $^{Cu}\Theta_{11}$ component is located along the Cu–N bond and $^{Cu}\Theta_{33}$ along the Cu–O bond, due to the lack of the ion–dipole interaction. The distortion of the electron density around the guest remains similar to that obtained for **1**-F, **1**-Cl, **1**-Br and **1**-I.

The observed variation in the local quadrupole moment at the host Cu(II) centers (Table 3) reveals that the inclusion of metallacycles as host species in the formation of host–guest pairs presents great advantages in comparison to their organic counterparts. This is prompted by the large versatility provided by the metallic centers to the host (Cu, in our case), that can vary their electron densities according to the involved guest, leading to different ranges of electron-density anisotropies ($\Theta_{aniso}$), associated with electron density fluctuations, and thus, with non-covalent interactions. Severin and coworkers based on a Mulliken population analysis found that in metallacrowns, oxygen atoms adjacent to metallic centers present more negative charges in comparison to those belonging to similar crown ethers, reflecting the high polarization of metal–oxygen bonds in this kind of systems.[52]

### Non-covalent interaction index

In 2010 Johnson[53] and coworkers proposed a descriptor for non-covalent interactions (NCI), based on the reduced density gradient ($s$) at low density regions ($\rho$). This analysis provides a graphical index, which allows the characterization of the

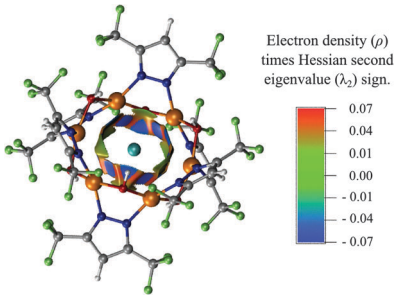


Fig. 5 NCI analysis of [*trans*-$Cu_6\{\mu$-3,5-$(CF_3)_2pz\}_6(\mu$-$OH)_6Cl]^-$.

binding forces within the host–guest pair. The reduced density gradient is given by

$$s = \frac{1}{2(3\pi^2)^{1/3}} \frac{\nabla\rho}{\rho^{4/3}}$$

The reduced density gradient at low density regions verifies the presence of non-covalent interactions. Each point in this region is correlated with the second eigenvalue of the electron density Hessian ($\lambda_2$) times the electron density. The values of $\lambda_2$ give information about the type of binding force: attractive forces, such as hydrogen bonds ($\lambda_2 < 0$), weak interactions ($\lambda_2 \approx 0$) or repulsive forces ($\lambda_2 > 0$).[27] The analysis of non-covalent interactions for [*trans*-$Cu_6\{\mu$-3,5-$(CF_3)_2pz\}_6(\mu$-$OH)_6Cl]^-$ is presented in Fig. 5, where a region involving non-covalent interactions is located between the $Cu_6$ ring and the central guest, which accounts for the interaction between the positive and negative components of the quadrupole tensor. Similar results are obtained with the rest of halide-complexes. As can be seen, hydrogen bonds occur between the halide ions and hydroxyl groups, where these forces also contribute to the stabilization of the complex.

### Through-the-space magnetic response

The metallacycle, *trans*-$Cu_6\{\mu$-$(3,5$-$(CF_3)_2pz)\}_6(\mu$-$OH)_6$ (**1**), exhibits a singlet spin ($S = 0$) ground state where the Cu(II) centers are coupled antiferromagnetically, as it is observed for **1**-Cl[17] and for the isostructructural [*trans*-$Cu_6\{\mu$-3,5-$(CH_3)_2pz\}_6$-$(\mu$-$OH)_6\cdot CH_3CN\cdot CHCl_3]$[8] in agreement to our calculations.

The singlet ground state of **1** enables a clear evaluation of the magnetic response, which provides a sensitive and powerful tool to account for the chemical environment. In this sense, NMR experiments have been widely employed in the description of host–guest systems where the formation of the host–guest pair induces a modification in the respective chemical shift in comparison to the isolated form.[54] In addition to the chemical shift tensor centered at each atom, accounting for the NMR experiments,[55,56] the overall magnetic response can be conveniently generalized through the space. This leads to a graphical representation of the short- and long-range magnetic behavior driven by the presence of induced currents.[57,58] Hence, with the aim of gaining a deeper understanding of the magnetic response of **1**, and how the inclusion of a given guest

 

modifies this behavior, we describe the molecular response under a uniform external magnetic field ($\boldsymbol{B}^{ext}$) by mapping the induced magnetic field ($\boldsymbol{B}^{ind}$) quantity for **1** and **1**-Cl. Such terms are related to the second-rank shielding tensor ($\sigma_{ij}$) expressed in ppm units, according to the expression, $\boldsymbol{B}_j^{ind} = \sigma_{ij}\boldsymbol{B}_i^{ext}$,[55,56] which can be described in terms of the more familiar chemical shift tensor ($\delta_{ij}$), given by $\delta = (\sigma^{ref} - \sigma)/(1 - \sigma) \approx \sigma^{ref} - \sigma$.[55,56] For a nucleus-independent probe, $\sigma^{ref}$ is equal to zero, resulting in a relationship for each component of such tensor, given by $\delta_{ij} = -\sigma_{ij}$.[55,56] The i and j subindices are conveniently related to the *x*-, *y*- and *z*-axes of a molecule-fixed Cartesian system, instead of the principal axis system (PAS) for each nuclear independent point. The positive and negative values denote paratropic and diatropic induced currents,[55,56] respectively.

The isotropic term, $\delta_{iso}$, is related to the averaged magnetic response under different orientations of the applied field, resembling the tumbling of the molecule in solution as occurs in normal NMR experiments. The term $\delta_{iso}$ (Fig. 6) suggests the short range behavior of the induced currents in the *xy*-plane which are confined to the contour of the $Cu_6$ ring, leading to a small average response at its center ($< \sim 2$ ppm, usually described as NICS(0)). Thus, the magnetic response of an incoming guest will not be altered to a large extent, in contrast to other metallacycle cases.[58] The contribution to the averaged molecular response from each Cu(II) center is within the van der Waals radii (1.4 Å),[45] supporting the rather small direct interaction between such centers due to their Cu–Cu distance of 3.187 Å. Thus, it is clear that the coupling leading to the antiferromagnetic behavior is given by the superexchange interaction mediated by the ligands.

The analysis of certain components of the tensor describing the through-the-space magnetic response ($\delta$), offers a deeper understanding of the axis dependent magnetic response, denoting the magnetic complexity in this two dimensional structure.[42,57,58] The $\delta_{zz}$ component of the shielding tensor has been extensively used to characterize theoretically the presence of diatropic or paratropic induced ring currents[59,60] leading to shielded or deshielded regions, respectively. According to the magnetic criteria of aromaticity,[59,60] the shielding regions inside the $Cu_6$ ring can be directly related to a ring current effect[61,62] denoted by the shielding of $-7.36$ ppm under a perpendicular field in the center of the metallacycle. (The $\delta_{zz}$ component is also described as $NICS_{zz}(0)$.) It is noteworthy that as a consequence of the strong antiferromagnetic coupling between the Cu(II) centers driven by the superexchange through the ligands, a highly aromatic behavior is described. This behavior is intriguing, because it arises from the superexchange involving the ligands rather than a direct exchange between the Cu(II) centers. The path that leads to the here characterized aromatic behavior is currently under study in order to describe the contribution of the N–N or OH bridges to the superexchange and the aromatic character of **1**.

The formation of the host–guest complex (**1**-Cl) does not modify substantially the $\delta_{iso}$ of the isolated host, as a consequence of the short-range behavior observed. However, the $\delta_{zz}$ component denotes a stronger variation due to the presence of $Cl^-$, which gives rise to a large decrease of the diatropic currents at the Cu–Cl bond-critical-point (BCP) distances, as is obtained from the atoms-in-molecules theory (Fig. S2, ESI†). The decrease at such point from $-8.39$ ppm to $-0.44$ ppm could be attributed to the almost closed shell configuration of $Cl^-$ which contributes destructively to the diatropic currents associated with the aromatic behavior of **1**. However, upon the formation of the host–guest pair, the strong antiferromagnetic coupling between the six Cu(II) centers remains unaltered.[17]

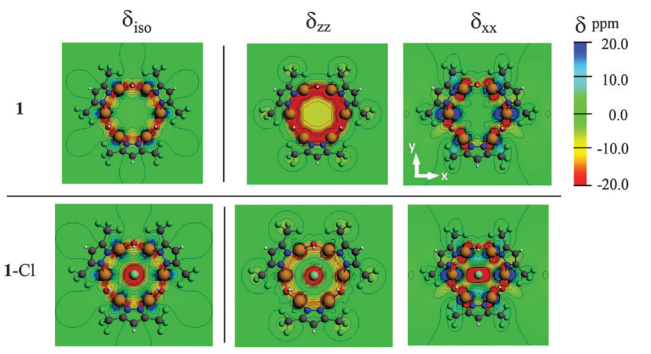


Fig. 6 Chemical shift map over the molecular domain, denoting the $\delta_{iso}$, $\delta_{zz}$ and $\delta_{xx}$ components. The molecule-fixed Cartesian coordinate system taken as a frame of reference is shown.

## Conclusions

The non-covalent forces in the host–guest systems involving the hexanuclear copper(II) pyrazolate complexes and a halide guest ($F^-$, $Cl^-$, $Br^-$, $I^-$), describe an ionic character ($\sim$70% of the stabilizing terms) whereas the dispersion term contributes to a rather small extent ($\sim$5%).

The evaluation of the hypothetical noble-gas counterparts allows us to obtain a case for comparison, where the electrostatic term of the stabilizing energy is highly quenched, allowing to evaluate the contribution of the ion–dipole interaction to the overall host–guest formation. According to our results, the ion–dipole contribution to the stabilizing electrostatic term ranges from 95.0% to 77.0% going from **1**-F to **1**-I, describing the increasing role of higher order interactions such as quadrupole–dipole and quadrupole–quadrupole in the host–guest pair formation. Our results suggest that the interaction with a softer guest increases the contribution from higher order interactions.

According to the inclusion of a given halide ion, the local dipole moment and the local electric quadrupole moment of the host binding sites, namely Cu(II), vary in different amounts. Thus, this observed variation in the quadrupole and dipole moments at host Cu centers, reveals that the inclusion of metallacycles as host species in the formation of host–guest pairs presents great advantages from its organic counterparts, because such centers can modulate their electron density to a considerable extent in order to maximize the host–guest interaction. The graphical representation of the local quadrupole moments ($\Theta$) describes that the electron-deficient regions above and below the $Cu_6$ plane are those that mainly interact

with the negative axial distribution of the guest, leading to the rise of quadrupole–quadrupole host–guest forces, which increase as $\Theta_{aniso}$ goes towards more negative values, as occurs in the **1**-I case. Our methodology involving the graphical representation of $\Theta$, offers a clear representation of high-order interactions. Hence, ion–dipole and quadrupole–dipole interactions are located at the $Cu_6$ ring plane, whereas quadrupole–quadrupole interactions are located mainly above and below such plane.

Noteworthy, the magnetic behavior of **1** reveals a highly aromatic structure. This point exhibits the aromatic behavior driven by the superexchange through the ligands, in addition to the usual aromatic species where a direct interaction between the neighbour centers is present. The path that leads to the here characterized aromatic behavior is currently under study in order to describe the contribution of the N–N or OH bridges to the superexchange and aromatic character of **1**.

## Acknowledgements

The author thanks for financial support from FONDECYT Grant 1140359 and PROJECT MILLENNIUM RC120001. M.P.-V. acknowledge Conicyt doctoral fellowships.

## Notes and references

1 R. Galassi, A. Burini and A. Mohamed, *Eur. J. Inorg. Chem.*, 2012, 3257.
2 B. Gibney, H. Wang, J. Kampf and V. Pecoraro, *Inorg. Chem.*, 1996, **35**, 6184.
3 G. Ardizzoia, S. Cenini, G. La Monica, N. Masciocchi and M. Moret, *Inorg. Chem.*, 1994, **33**, 1458.
4 M. Tanabe and K. Osakada, *Organometallics*, 2010, **29**, 4702.
5 C. M. Zaleski, S. Tricard, E. C. Depperman, W. Wernsdorfer, T. Mallah, M. L. Kirk and V. Pecoraro, *Inorg. Chem.*, 2011, **50**, 11348.
6 M. Alexiou, I. Tsivikas, C. Dendrinou-Samara, A. Pantazaki, P. Trikalitis, N. Lalioti, D. Kyriakidis and D. Kessissoglou, *J. Inorg. Biochem.*, 2003, **93**, 256.
7 P. Thanasekaran, C. Lee and K. Lu, *Acc. Chem. Res.*, 2012, **45**, 1403.
8 W. Cañón-Mancisidor, C. J. Gómez-García, G. Mínguez Espallargas, A. Vega, E. Spodine, D. Venegas-Yazigi and E. Coronado, *Chem. Sci.*, 2014, **5**, 324.
9 G. L. Abbati, A. Cornia, A. C. Fabretti, W. Malavasi, L. Schenetti, A. Caneschi and D. Gatteschi, *Inorg. Chem.*, 1997, **36**, 6443.
10 U. Patel, H. Singh and G. Wolmershäuser, *Angew. Chem.*, 2005, **117**, 1743.
11 J. A. Halfen, J. J. Boldwin and V. Pecoraro, *Inorg. Chem.*, 1998, **37**, 5416.
12 S. K. Mandal, V. G. Young and L. Que, *Inorg. Chem.*, 2000, **39**, 1831.
13 J. T. Grant, J. Jankolovits and V. Pecoraro, *Inorg. Chem.*, 2012, **51**, 8034.
14 D. P. Goldberg, S. Michel, A. White, D. J. Williams, A. Barrett and B. M. Hoffman, *Inorg. Chem.*, 1998, **37**, 2100.
15 G. A. Ozin and A. C. Arsenault, *Nanochemistry: A Chemical Approach to nanomaterials*, Royal Society of Chemistry, Cambridge, 2005.
16 R. D. Adams and F. A. Cotton, *Catalysis by Di- and Polynuclear Metal Cluster Complexes*, Wiley-VCH, New York, 1998.
17 A. Mohamed, S. Ricci, A. Burini, R. Galassi, C. Santini, G. Chiarella, D. Melgarejo and J. Fackler, *Inorg. Chem.*, 2011, **50**, 1014.
18 R. G. Pearson, *Chemical Hardness: Applications from Molecules to Solids*, Wiley-VCH, Weinheim, 1997.
19 D. Reger, E. Fole and M. Smith, *Inorg. Chem.*, 2009, **48**, 936–945.
20 F. Z. London, *Physik*, 1930, **63**, 245.
21 M. Kolář, T. Kubař and P. Hobza, *J. Phys. Chem. B*, 2011, **115**, 8038.
22 S. Grimme, *Wiley Interdiscip. Rev.: Comput. Mol. Sci.*, 2011, **1**, 211.
23 S. N. Steinmann and C. Corminboeuf, *J. Chem. Theory Comput.*, 2011, **7**, 3567.
24 M. Swart, P. Van Duijnen and J. G. Snidjers, *J. Comput. Chem.*, 2001, **22**, 79.
25 J. Hernández-Trujillo, *J. Phys. Chem.*, 1996, **100**, 6524.
26 J. Hernández-Trujillo and A. Vela, *J. Chem. Soc., Faraday Trans.*, 1993, **89**(14), 2441.
27 J. Contreras-García, E. R. Johnson, S. Keinan, R. Chaudret, J. Piquemal, D. N. Beratan and W. Yang, *J. Chem. Theory Comput.*, 2011, **7**(3), 625.
28 R. Parr and W. Yang, *Density Functional Theory of Atoms and Molecules*, Oxford University Press, New York, 1989.
29 Amsterdam Density Functional (ADF) code. Release 2012, Vrije Universiteit, Amsterdam, Netherlands.
30 J. Tao, J. P. Perdew, V. N. Staroverov and G. E. Scuseria, *Phys. Rev. Lett.*, 2003, **91**(14), 146401.
31 V. N. Staroverov and G. E. Scuseria, *J. Chem. Phys.*, 2003, **119**(23), 12129.
32 Y. Zhao and D. G. Truhlar, *J. Chem. Phys.*, 2006, **124**, 224105.
33 J. Tao, S. Tretiak and J. Zhu, *J. Chem. Phys.*, 2008, **128**(8), 084110.
34 L. Verluis and T. Ziegler, *J. Chem. Phys.*, 1988, **88**, 322.
35 A. Mohamed, A. Burini, R. Galassi, D. Paglialunga, J. Galán-Mascarós, K. Dunbar and P. Fackler, *Inorg. Chem.*, 2007, **46**(7), 2348.
36 E. Zurek, C. J. Pickard and J. Autschbach, *J. Phys. Chem. C*, 2008, **112**, 11744.
37 A. Muñoz-Castro, *Chem. Phys. Lett.*, 2013, **555**, 282.
38 G. A. Zhurko, http://www.chemcraftprog.com.
39 G. Saleh, C. Gatti and L. Lo Presti, *Comput. Theor. Chem.*, 2012, **998**(15), 148.
40 G. Saleh, C. Gatti, L. Lo Presti and J. Contreras-García, *Chem. – Eur. J.*, 2012, **18**, 15523.
41 W. Humphrey, A. Dalke and K. Schulten, *J. Mol. Graphics*, 1996, **14**(1), 33.
42 S. Klod and E. Kleinpeter, *J. Chem. Soc., Perkin Trans. 2*, 2001, 1893.
43 N. C. Handy and A. J. Cohen, *Mol. Phys.*, 2001, **99**, 403.
44 J. P. Perdew, K. Burke and M. Ernzerhof, *Phys. Rev. Lett.*, 1996, **77**, 3865.

 

45 A. Bondi, *J. Phys. Chem.*, 1964, **68**(3), 441.
46 K. Morokuma, *J. Chem. Phys.*, 1971, **55**, 1236.
47 A. D. Buckingham, *Chem. Rev.*, 1988, **88**, 963.
48 B. Le Guennic and J. Autschbach, *Can. J. Chem.*, 2011, **89**, 814.
49 R. Bader and C. Chang, *J. Phys. Chem.*, 1989, **93**, 2946–2956.
50 K. J. D. MacKenzie and M. E. Smith, *Multinuclear Solid-State NMR of Inorganic Materials*, Elsevier, Oxford, 2002.
51 U. Haeberlen, *High resolution NMR in solids: Selective averaging*, Academic Press, New York, 1976.
52 M. Lehaire, A. Schulz, R. Scopelliti and K. Severin, *Inorg. Chem.*, 2003, **42**, 3576.
53 E. R. Johnson, S. Keinan, P. Mori-Sanchez, J. Contreras-Garcia, A. J. Cohen and W. Yang, *J. Am. Chem. Soc.*, 2010, **132**, 6498.
54 F. Ziarelli and S. Caldarelli, *Solid State NMR*, 2006, **29**, 214.
55 R. S. Drago, *Physical Methods in Chemistry*, W.B. Saunders, Philadelphia, 1977, ch. VII.
56 M. Kaupp, M. Bühl and V. G. Malkin, *Calculation of NMR and EPR Parameters. Theory and Applications*, Wiley-VCH, Weinheim, 2004.
57 R. Guajardo, M. Ponce Vargas and A. Muñoz-Castro, *J. Phys. Chem. A*, 2012, **116**, 8737.
58 A. Muñoz-Castro, *J. Phys. Chem. C*, 2012, **116**, 17197.
59 P. v. R. Schleyer and H. Jiao, *Pure Appl. Chem.*, 1996, **68**, 209.
60 P. Lazzeretti, *Phys. Chem. Chem. Phys.*, 2004, **6**, 217.
61 T. Haine, C. Corminboeuf and G. Sifert, *Chem. Rev.*, 2005, **105**, 3889.
62 G. Merino, T. Heine and G. Seifert, *Chem. – Eur. J.*, 2004, **10**, 4367.